A NOVEL PIPE-CLIMBING FLEXIBLE ROBOT FOR PIPE INSPECTIONS

Minh Hoan Vu[1,*], Xuan Hiep Trinh[1], Van Hoan Nguyen[1]

[1]*Faculty of Mechanical Engineering, Le Quy Don Technical University*

Abstract

For robots, crawling through curved or redirected pipe sections with different pipe diameters to inspect and survey pipes is quite a difficult task. To solve this problem, in this article we propose a new pipe inspection robot model that is a combination of rigid mechanical structures with a soft body to ensure the robot moves smoothly and is flexible. The mechanical design model of the robot includes the front radial actuator, the central axial actuator, and the rear radial actuator. In order to assist the robot in adhering tightly to the pipe wall and producing a fulcrum for stable movement, the front and rear actuators are made of a rigid mechanical framework that can expand radially. The central axial actuator is the soft body that can flow through curved pipes and expand rapidly in the axial direction when filled with air to aid in the robot's forward motion. The robot's flexibility in movement is made clear by kinematic models of mechanical structures and deformation simulations of soft bodies. Preliminary calculations and simulation results show that this new robot design has the potential to move flexibly and efficiently in pipes with variable diameters and diverse configurations.

Keywords: *Crawling robot; flexible robot; mechanical design; kinematic model.*

1. Introduction

Robots have become an indispensable part of people's lives. Robots replace humans to do heavy and dangerous jobs. For instance, assessing and surveying subterranean pipeline systems is necessary to minimize damage and repair time via early detection of accidents and damage inside the pipeline. Over time of use, pipes are susceptible to defects such as corrosion, stress, and aging that cause pipes to leak, crack, or break. As a result, it is possible to slow down the decrease in business activity, which will have a significant effect on the oil and gas industry [1, 2]. In addition, as a tiny robot can climb into chimneys and pipes to look for survivors, pipe-climbing robots can also be utilized for search and rescue operations [3-5]. Due to their high practicality, pipeline inspection robots have played an important role in recent years and have become an urgent need in society.

Many pipeline inspection robots have been proposed in the past two decades based on wheeled, caterpillar, snake, legged, worm, screw, helical drive [6], and other specific

[*] Corresponding author, email: hoanvm@lqdtu.edu.vn
DOI: 10.56651/lqdtu.jst.v19.n03.811

structure types [7, 8]. To move through the pipeline, these robots must continuously operate under the high pressure of the fluid flow, changing their outer diameter and switching from horizontal crawling to vertical climbing. Basic climbing ability has been reported in wave robots [4, 5], deep robots [9, 10], and robots that rely on friction to climb [11, 12]. However, these robots are not designed to significantly change their diameter to adapt to different pipe diameters, make turns along the curvature of the pipe, or switch from horizontal crawling to vertical climbing. Snake robots [12, 13] have the ability to alter their outward shape in order to adapt to varying pipe diameters. They can also move forward by using several gaits while crawling through pipe branches. However, they move forward by sliding, which consumes energy and limits their mobility. In order to increase their outside diameter, these robots are constructed with many joints. Robots with different moving methods are presented in [14-17], such as helical drive [15, 16] and the two-mass inertial method [17]. The pipe-climbing robots mentioned above often have a rigid mechanical structure. The advantages of this type of robot are high durability, good bearing capacity, stable movement, and great accuracy in measurement and inspection duties. This kind of robot's drawback is that it is less flexible when navigating through intricately shaped pipes, tiny curved angles, or pipe sections with varying diameters. In addition, this robot often has a large size, weight, and complex mechanical structure, so it is only suitable for moving large-diameter pipes.

In recent years, there has been a significant increase in the study and use of soft robot structures due to their flexibility and softness. Soft robots are also widely utilized in many other fields, particularly in the areas of harmful environment pipeline surveying and inspection, as well as human blood vessel and intestinal examination. Soft robots are capable of operating independently and flexibly by using highly elastic materials for the main body and moving parts [18, 19], such as polymers, silicone rubber, or other types of soft materials [20]. Unlike rigid manipulators, soft robots are considered to have infinite degrees of freedom because they can deform arbitrarily [21, 22], are suitable for various complex environments, and can interact safely with objects when they come into contact [23]. In addition, soft robots can easily access narrow spaces, curved roads, and deformed pipes. However, the structure of this type of robot is often made of a soft body that is easily deformed, so its bearing capacity is small, there is less stable movement and lower energy efficiency, and its load-carrying capacity is small, so this type of robot is often only suitable for pipes with small diameters of a few tens of centimeters or less. The publication [24] provides a summary of pipe-climbing robot models, which are typically designed based on either rigid or soft body structures but not a combination of these mechanisms. This limitation restricts the flexibility and performance of the robots. Additionally, a mix of soft and hard

constructions for worm-like in-pipe robots was presented in [25]. The center motion actuator in this design is a stiff structure, whereas the robot's front and rear actuators are made of extremely elastic materials. The robot can only move in pipe sections with a certain diameter because soft actuators at both ends are used to generate friction with the pipe wall. Furthermore, the robot's front and rear actuators exert very little force on the tube wall, which results in a low level of stable moving capability. Additionally, this design restricts the robot's capacity to maneuver through curved pipes because the central actuator is a hard structure.

Because of the drawbacks and restrictions of every kind of robot and to address the need for more flexible movement within complex pipeline systems, it is an urgent requirement to design a new robot model that addresses the current technical requirements. In this article, we introduce a novel flexible robot design that combines the strengths of both rigid and soft structures. The robot has a rigid frame structure that can expand radially to help the robot adhere tightly to the pipe wall, and the center soft body has the ability to flexibly stretch to help the robot move forward and adapt through sections of curved tube. With this structure, the robot has both high rigidity and the ability to move smoothly, stably, and flexibly in pipes with variable diameters and different directions of movement. This is a new potential solution to using this kind of robot for surveying and inspecting pipeline systems.

2. Design and movement of the flexible robot

2.1. Design of the flexible robot

This robot design model aims to allow the robot to move flexibly in straight pipe segments of varying diameters. As shown in Fig. 1, the flexible robot includes a front radial actuator (1), a central axial actuator (2), and a rear radial actuator (3). All three actuators are driven by compressed air through air ducting (4). The front (1) and rear (3) radial actuators of the robot will expand axially after inflation, resulting in the radial movement of the friction plate (6) (shown in Fig. 2). The central axial actuator (2) can expand in the axial direction and limit radial expansion after being injected with air. By alternately inflating and deflating the three actuators, the robot will crawl forward into the tube. As shown in Fig. 2, the construction of the front actuator and the rear actuator are similar. The initial diameter and length of these two actuators are 73 mm and 56 mm, respectively; the initial diameter and length of the central shaft drive are 35 mm and 80 mm, respectively (Fig. 3). The air chambers of the actuators are made of highly elastic silicone rubber material, with a wall thickness of 2 mm. The material of the remainder parts of the robot is steel. In particular, springs are made from carbon-steel materials. The

robot measures about 284 mm in length and 73 mm in diameter, and its weight is about 1.85 kg, which can be estimated based on the robot's 3D model in Inventor software (Fig. 1).

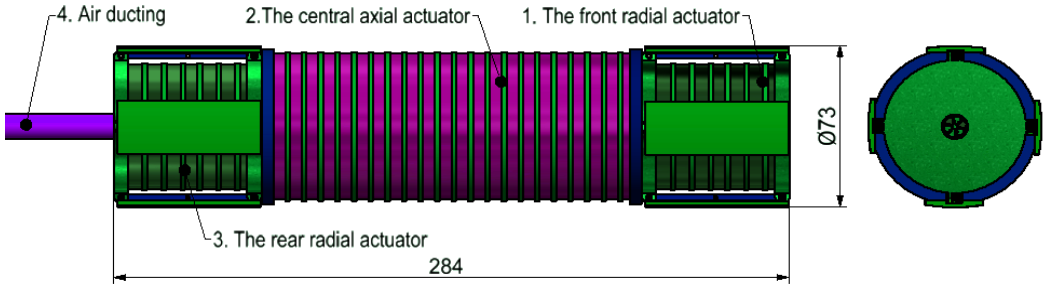

Fig. 1. The structure and size of the flexible robot.

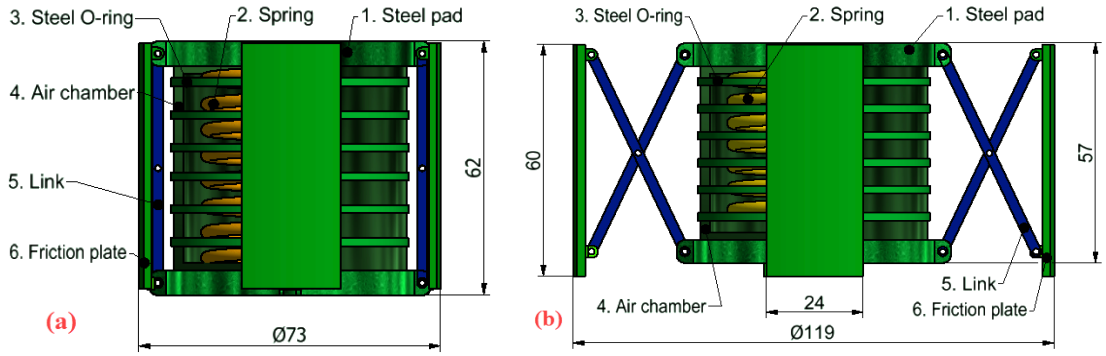

Fig. 2. Structure of the front and rear radial actuators
a) The initial state of the radial actuator; b) The state of the radial actuator after deflation.

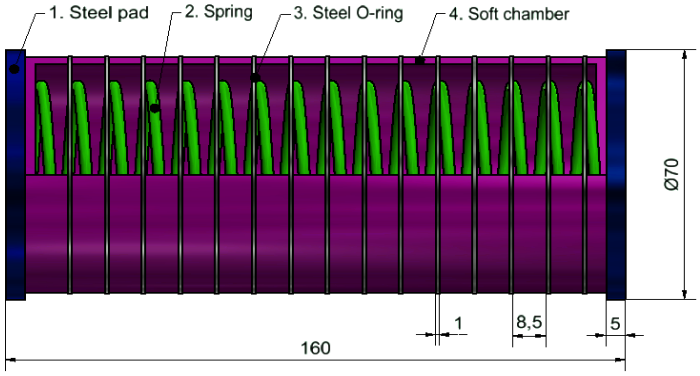

Fig. 3. The structure and size of the central axial actuator.

2.2. Movement of the flexible robot

Figure 4 shows the entire motion cycle of the flexible robot in the pipeline, where Fig. 4a is the initial state of the robot and Figs. 4b - 4f are five different motion states of the robot. At first, the rear radial actuator will be discharged, and the air chamber will collapse under the elastic force of the spring and the pressure difference inside and outside

the air chamber. This movement will drive the steel pad (1), which is connected to the friction plate (6) through the transmission links (5). The movement of the steel pad (1) causes the friction plate (6) to open in the radial direction and press against the inner wall of the tube, creating a stable fulcrum. Thus ensuring the robot does not move backward when the central actuator is pumped with air (Fig. 4b). Next, the central actuator is pumped with air, causing it to expand in the direction of the robot's axis, pushing the radial actuator (1) forward (Fig. 4c). Then, the front radial actuator (1) is released with the air, and the air chamber is collapsed under the effect of spring elasticity and the pressure difference inside and outside the air chamber. This movement causes the friction plate (6) to move radially via the movement of the steel pad (1) (the front and rear radial actuators operate on the exact same principle), causing the friction plate (6) to press close to the inner wall of the tube (Fig. 4d), creating a solid fulcrum for the robot, and at the same time, the rear radial actuator is pumped with air to narrow the diameter of the friction plates, returning the rear radial actuator to a free state. Then, the central axial actuator is deflated (Fig. 4e), and under the elastic force of the spring at the central actuator (2), the rear radial actuator (3) is pulled towards the front. Finally, the rear radial actuator is released with air, expanding the friction plates against the inner wall of the tube (Fig. 4f), and meanwhile, the front radial actuator is brought to a relaxed state by the air pump, and the flexible robot in the tube returns to its original state, ending one cycle of robot movement. The robot repeats this cycle to keep it moving forward. In addition, the robot will move backwards if the entire above process is reversed.

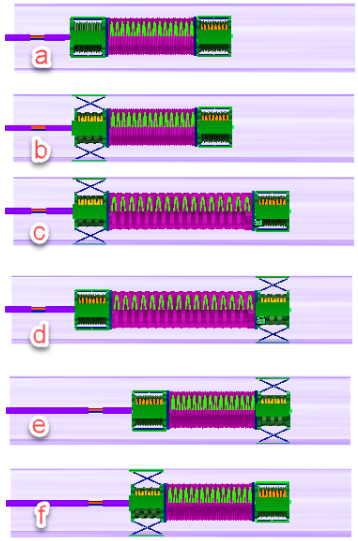

Fig. 4. A movement cycle of the flexible robot

(a) The initial state of the flexible robot; (b-f) Five statuses during the movement.

3. Numerical simulation of the flexible robot

3.1. The kinematic model of a radial actuator

The diagram of the force acting on the radial actuator is illustrated in Fig. 5, and Table 1 provides the values of radial actuator's kinematic parameters.

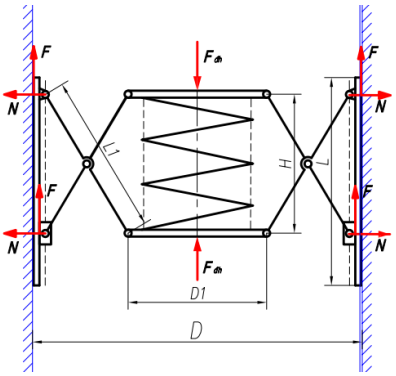

Fig. 5. Forces applied to a radial actuator after deflation.

Tab. 1. Kinematics parameters of the radial actuator

D (mm)	D_1 (mm)	L_1 (mm)	μ
119	73	56	0.7

The reaction force and friction force acting on the pipe wall caused by the friction plate are calculated according to the following formulas:

$$N = \frac{k(D-D_1)\left(\sqrt{L_1^{\,2} - \frac{(D-D_1)^2}{4}} - S_0\right)}{2\sqrt{L_1^{\,2} - \frac{(D-D_1)^2}{4}}} \quad ; \quad F = \mu N \tag{1}$$

where N is the force exerted on the pipe wall by the friction plate, k is the spring stiffness, S_0 is the initial length of the spring, L_1 is the connecting rod length, D is the pipe diameter, D_1 is the diameter of the steel pad, μ is the friction coefficient, F is the friction force caused by the friction plate. Here, we can select a friction coefficient of 0.7, assuming that the tube's surface is dry and clean, because the contact between the friction plate and the pipe wall is the contact of a steel-steel material pair with a static friction coefficient in the range of 0.7 - 0.74.

The friction force and reaction force change as the spring's initial stiffness and length are altered, as seen in Fig. 5 and Fig. 6.

As we can see in Fig. 5, we see that when the pipe diameter D changes, the friction force of the robot acting on the pipe wall also changes. By altering the air pressure pumped into the air chamber, we can modify the initial length H and make sure the robot

adheres tightly to the pipe wall while it moves. Fig. 6 and Fig. 7 show us that the friction force acting on the tube wall depends on the initial length and stiffness of the spring. Therefore, we can choose the size and hardness of the spring to match the structure of the robot during the design process. We can choose the working pressure range in the air chamber under actual conditions to ensure the robot moves stably and smoothly. Furthermore, make sure the robot moves steadily in the event that the pipe is vertical (Fig. 8).

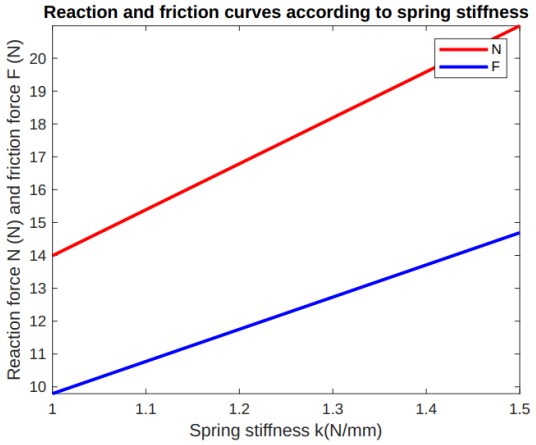

Fig. 6. Reaction and friction force variations based on spring stiffness.

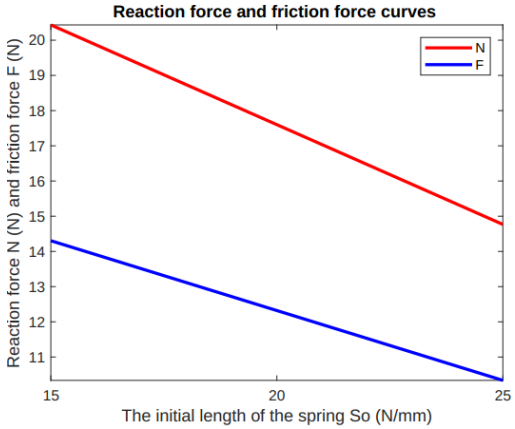

Fig. 7. Reaction force and friction force variations based on spring length initialization.

Fig. 8. The robot moves in a vertical tube.

Change in diameter of the radial actuator is calculated according to the following formulas:

$$D = D_1 + 2\sqrt{x(2L_1 - x)} \tag{2}$$

where D is the diameter of the radial actuator after expansion, which is the same as the required pipe's diameter, x is the displacement of the steel pad (1) along the robot's axis (Fig. 9).

The kinematic model of the radial actuator is illustrated in Fig. 9, and the change in diameter of the radial actuator after deflation is shown in Fig. 10.

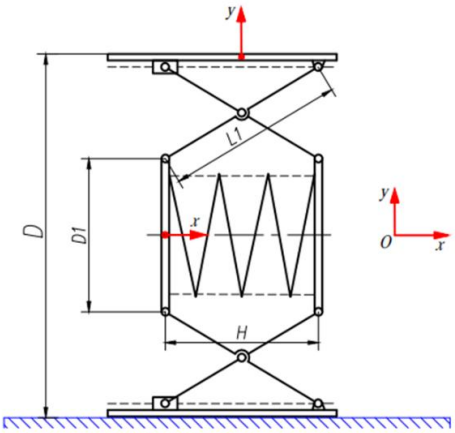

Fig. 9. The kinematic model of the actuator.

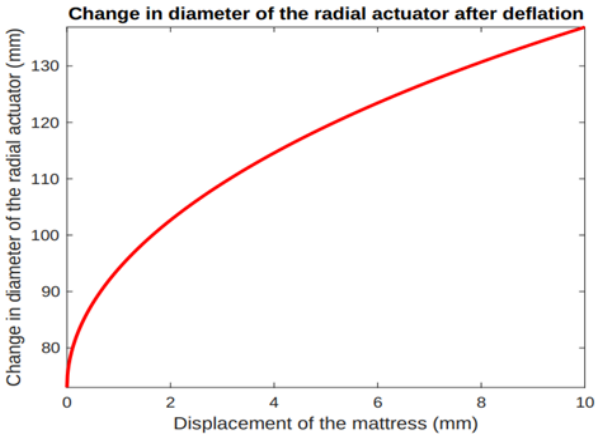

Fig. 10. Change in diameter of the radial actuator after deflation.

As shown in Fig. 9, when the robot moves in a pipe with a variable diameter, the displacement distance of the steel plate (1) changes, which will change the diameter of the radial actuator *D*, causing the friction plate to be constantly pressed close to the tube wall. The optimality of the suggested structure is demonstrated by the substantial expansion of the diameter that is produced by a little movement of the mattress (Fig. 10). Furthermore, the structure of the radial actuator allows it to change diameter flexibly and quickly, thereby helping the robot move through pipes with different diameters (Fig. 11). Through calculation and simulation results, it shows that pipe sections of different sizes that the robot moves through will correspond to different levels of activated air pressure, as shown in Tab. 2.

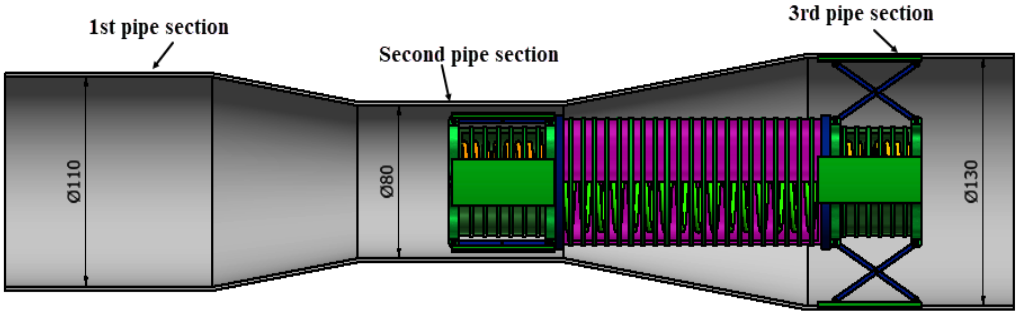

Fig. 11. The robot passes through pipelines with varying diameters.

Table 2. Pressure parameters in the air chamber of the front and rear actuators when the robot moves in 3 different pipe sections

	1st pipe section	2nd pipe section	3rd pipe section
Minimum air pressure in the air chamber	0.05 MPa	0.0017 MPa	0.123 MPa
Maximum displacement of the mattress (1)	3.145 mm	0.11 mm	7.795 mm
Maximum diameter of the actuator	110 mm	80 mm	130 mm

3.2. Simulating the deformation of air chambers

Inventor software was chosen as the tool in this study. Here, the rubber-silicone material used to fabricate the deformation layer of the 3 air chambers is determined with the Young's modulus of 435 psi and Poisson's ratio of 0.49. The numerical simulation results of the radial actuator are shown in Fig. 12 and Fig. 13. Fig. 12 shows the simulation results of the inflated radial actuator, and it shows that the air chamber expands only in the axial direction but does not deform in the radial direction. Due to the effect of the steel O-rings, the diameter expansion of the radial actuator is due to the displacement of the pad, followed by the movement of the friction plate. In addition, the axial strain amplitude is linear with the input pressure, as shown in Fig. 13. The influence of the steel O-rings on the deformation of the air chamber is shown in Fig. 14. Fig. 14's simulation results demonstrate that the air chamber has the greatest axial deformation with a steel O-ring count of 4 (N = 4), while the radial deformation is minimal and falls within an acceptable range.

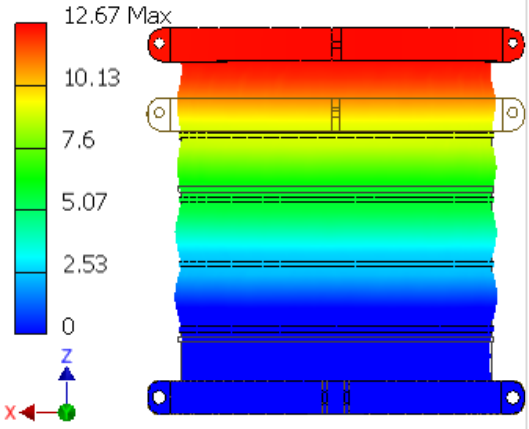

Fig. 12. Simulation result of the deformation of the radial actuator.

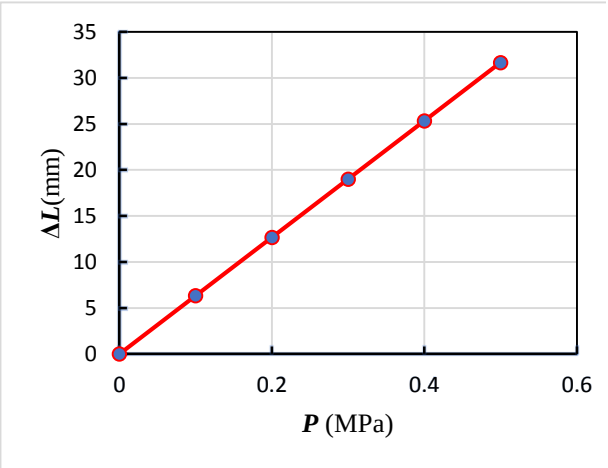

Fig. 13. Deformation-pressure curve of the radial actuator.

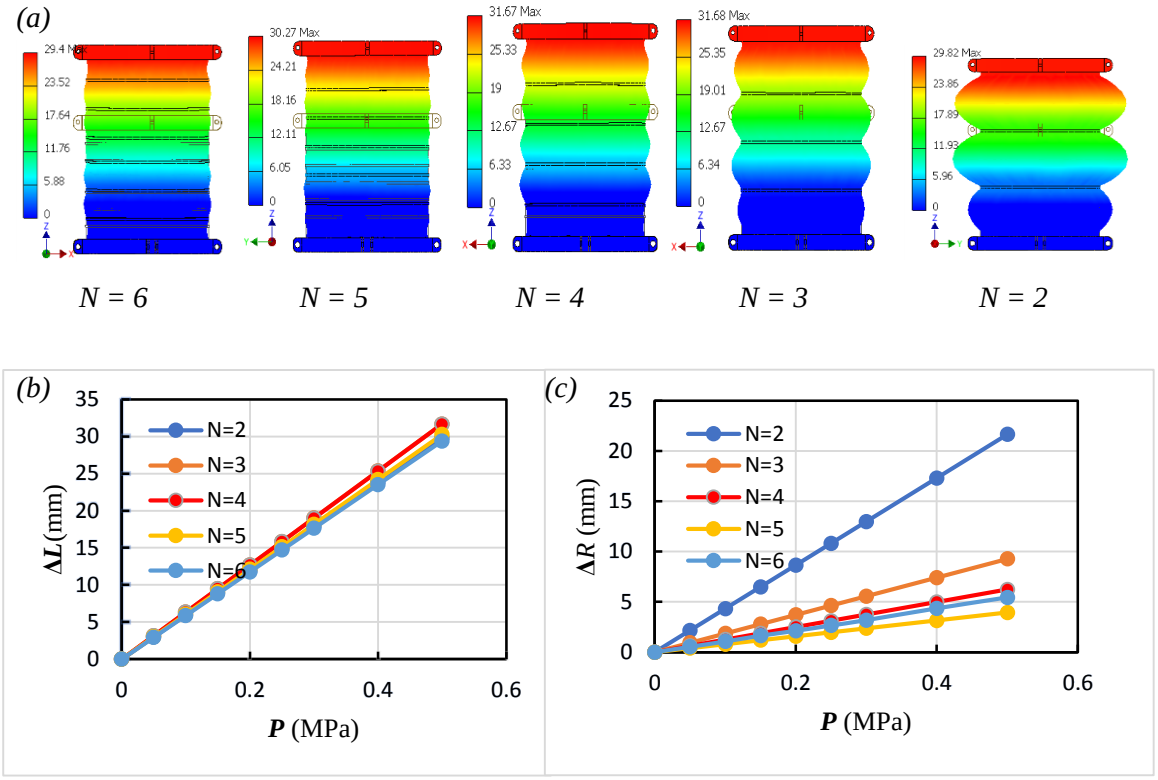

Fig. 14. The deformation of the air chamber in the radial actuator

a) Air chambers with different numbers of steel O-rings, N = 6, 5, 4, 3, and 2, respectively; b) The change of air chamber length L; c) The change of air chamber radius R, when the input air pressure changes from 0 to 0.5 MPa.

In addition, the numerical simulation results of the deformation of the axial actuator are shown in Fig. 15. Fig. 15's simulation results show that the actuator is only long out in the axial direction, but there is almost no deformation in the radial direction, through which we can see the effect of the O-rings surrounding the air chamber. The deformation results of the axial actuator alone with air pressure pushed into the air chamber, are displayed in Fig. 15a. The deformation results of the axial transmission under the influence of the elastic force of the spring situated in the air chamber, the weight of the radial transmission (0.6 kg), and the injected air pressure are depicted in Fig. 15b. The results demonstrate that there is little resistance from the weight of the radial actuator to the axial actuator's deformation, as evidenced by the minor actuator deformation difference between the two situations (Fig. 16). Furthermore, the influence of the steel O-rings on the deformation of the air chamber is shown in Fig. 17. The deformation of the central soft body creates translational motion for the robot, so it is necessary to investigate the influence of steel O-rings on the deformation of the soft body, thereby

determining the number of O-rings that is most suitable. To optimize the design of the robot, the number of steel O-rings must meet the following criteria: Firstly, ensure that the deformation of the soft body in the axial direction is maximum, which will increase the efficiency of the robot's movement. Secondly, the deformation in the radial direction is minimal; this will help the robot easily move through pipe sections with small diameters close to the diameter of the robot and, at the same time, increase the durability of the soft body because it does not overexpand during its operation.

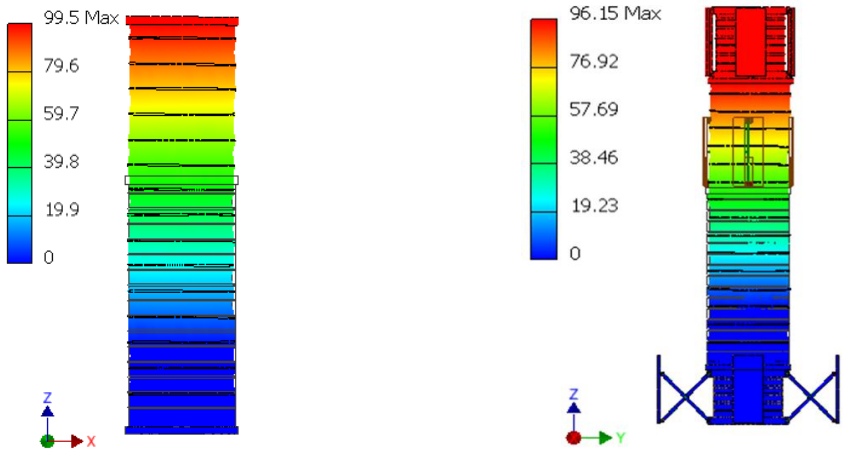

(a) *(b)*

Fig. 15. Simulation result of the deformation of the axial actuator

a) Simulation results of the deformation of the axial actuator; b) Simulation results of the deformation of the axial transmission under the gravity effect of the radial actuator.

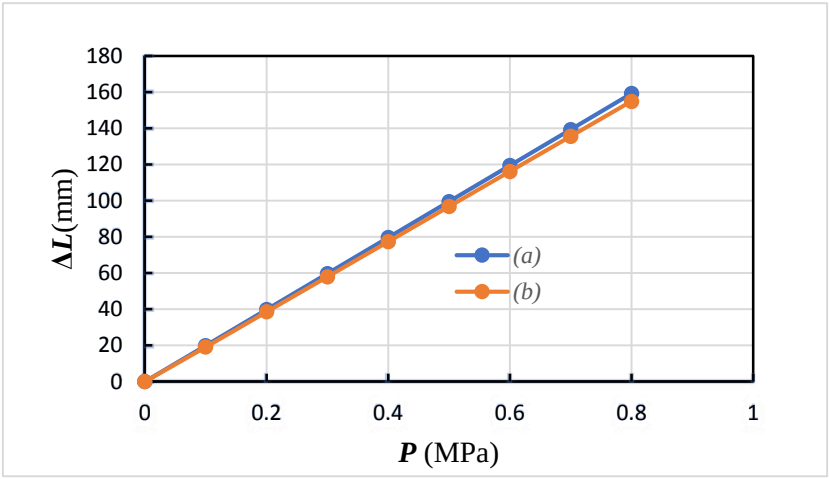

Fig. 16. Deformation-pressure curve of the axial actuator

a) Simulation results of the deformation of the axial actuator; b) Simulation results of the deformation of the axial transmission under the gravity effect of the radial actuator.

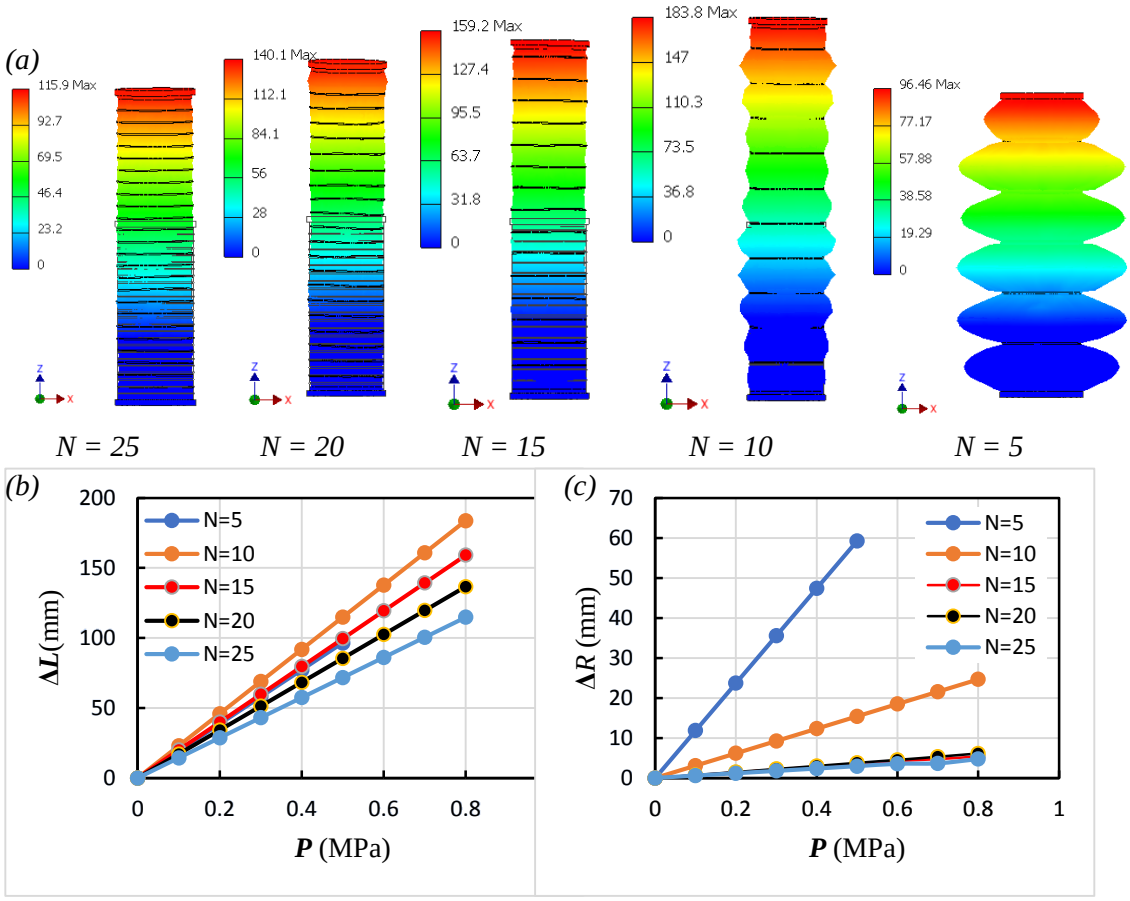

Fig. 17. The deformation of the air chamber in the axial actuator
a) Air chambers with different numbers of steel O-rings, N = 25, 20, 15, 10, and 5, respectively; b) The change of air chamber length L; c) The change of air chamber radius R, when the input air pressure changes from 0 to 0.8 MPa.

As shown in Fig. 17b and Fig. 17c the number of steel O-rings surrounding the air chamber has a direct effect on the deformation of the air chamber after being injected with air. It is clear that when we reduce the number of steel rings from 25 to 10, the axial deformation of the air chamber increases rapidly, however the radial expansion also increases but not much. Especially when continuing to reduce the number of steel rings to 5, the effect of axial deformation gradually decreases and is replaced by a rapid increase in radial deformation and the air chamber's structure is broken when the pressure increases to a larger extent 0.6 MPa. Most notable are the two cases where the number of O-rings is N = 10 and N = 15, and the deformation of the soft body in the axial direction is the largest and most effective in terms of robot movement. Specifically, with the number of O-rings N = 15, the axial deformation reaches 159.2 mm and the radial deformation reaches 7 mm at a pressure level of 0.8 MPa. With the number of O-rings

N = 10, the axial deformation reaches the maximum value of 183.2 mm (an increase of 15.45% compared to N = 10); however, the radial deformation reaches 26 mm (an increase of 271.42% compared to N = 10) at a pressure of 0.8 MPa. With the simulation results combined with the criteria for selecting O-rings stated above, we chose the number of steel O-rings on the axial actuator to be 15 (N = 15) during the process of completing the robot design.

4. Conclusion

To increase the softness of the robot moving through small and medium-diameter pipes (about 80 to 130 mm) and overcome the disadvantages of rigid robots, we presented a new flexible robot model design, which is a combination of radially expandable rigid mechanical structures and a soft body made of highly elastic material capable of expanding in the axial direction to help the robot move forward after being pumped with air. Additionally, the research has built a kinematic model for the robot's mechanical structures and simulated the deformation of the soft body parts of the robot using inventor software. The results of calculations and simulations indicate that this design model allows the robot's diameter to be freely changed between 80 and 130 mm, with the air chamber's pressure level ranging from 0.1 to 0.8 MPa. This will help the robot easily move through straight pipes with different diameter sizes. Furthermore, the friction force of the friction plate acting on the pipe wall can be changed by adjusting the pressure in the air chamber. From there, it can support the robot stick firmly to the pipe wall in a stable way during movement. However, this robot design model still has some limitations that need to be improved in future research. First of all, the robot is driven by compressed air which limits its travel distance as well as its low energy efficiency. This restriction can be addressed by applying the idea of magnetic fields or electric motor drives in place of pneumatic drives. Next, the robot's present configuration restricts its flexibility, particularly when maneuvering through intricately curved pipes with bend angles exceeding ninety degrees. Therefore, it is necessary to research the synchronous adjustment of the robot's structure in a different aspect or change the soft body structure from one cavity to many air chambers with different cross-sections, and at the same time combine pressure control in the cells in that cavity, which allows the soft body to bend along the curve of the tube.

In the future, we will further optimize the robot's structure to enable it to move more fluidly, easily, and efficiently in pipe sections that bend in different directions. Examples of these pipe sections include those with bends greater than 90 degrees, twisted pipes, and pipes with frequently changing diameters. In addition, it is necessary to further investigate the effect of friction between the friction plate and the pipe wall under

different working conditions, such as wet or dry pipes or pipes composed of various materials. Besides, a model to calculate the relationship between compressed air pressure and friction force on the pipe wall needs to be proposed, thereby perfecting the control method for the robot so that the robot can move more stably. At the same time, different robot designs need to be manufactured for testing to verify the results of theoretical calculations and its ability to operate in practice. In later research, we will attempt to address these concerns.

Acknowledgement

This research is funded by Le Quy Don Technical University Research Fund under the grant number 24.1.23.

References

[1] Md Raziq Asyraf Md Zin, Khairul Salleh Mohamed Sahari, Juniza Md Saad, Adzly Anuar, and Abd Talip Zulkarnain, "Development of a low cost small sized in-pipe robot", *Procedia Engineering*, Vol. 41, 2012, pp. 1469-1475. DOI: 10.1016/j.proeng.2012.07.337

[2] M. H. Skjelvareid, Y. Birkelund, and Y. Larsen, "Internal pipeline inspection using virtual source synthetic aperture ultrasound imaging", *NDT & E International*, Vol. 54, pp. 151-158, 2013. DOI: 10.1016/j.ndteint.2012.10.005

[3] Q. Xie, S. Liu, and X. Ma, "Design of a novel inchworm in-pipe robot based on cam-linkage mechanism", *Advances Mechnical Engineering*, Vol. 13, No. 9, pp. 1-11, 2021. DOI: 10.1177/ 16878140211045193

[4] D. Zarrouk, M. Mann, N. Degani *et al.*, "Single actuator wave-like robot (SAW): Design, modeling, and experiments", *Bioinspiration & Biomimetics*, Vol. 11, No. 4, 2016. DOI: 10.1088/1748-3190/11/4/046004

[5] A. Kernbaum, A. D. Horchler, K. M. Shaw, H. J. Chiel, and R. D. Quinn, "Worms, waves and robots", *Proceedings of the IEEE International Conference on Robotics and Automation*, Saint Paul, USA, 2012, pp. 3537-3538. DOI: 10.1109/ICRA.2012.6224805

[6] N. S. Roslin, A. Anuar, M. F. A. Jalal, and K. S. M. Sahari, "A review: Hybrid locomotion of in-pipe inspection robot", *Procedia Engineering*, Vol. 41, pp. 1456-1462, 2012. DOI: 10.1016/j.proeng.2012.07.335

[7] A. Kakogawa, Y. Oka, and S. Ma, "Multi-link articulated wheeled in-pipe robot with underactuated twisting joints", *Proceedings of the IEEE International Conference on Mechatronics and Automation (ICMA)*, Changchun, China, 2018, pp. 942-947. DOI: 10.1109/ICMA.2018.8484370

[8] S. Roh, D. W. Kim, J. S. Lee, H. Moon, and H. R. Choi, "In-pipe robot based on selective drive mechanism", *International Journal of Control, Automation and Systems*, Vol. 7, pp. 105-112, 2009. DOI: 10.1007/s12555-009-0113-z

[9] D. Zarrouk and M. Shoham, "Analysis and design of one degree of freedom worm robots for locomotion on rigid and compliant terrain", *ASME Journal of Mechanical Design*, Vol. 134, Iss. 2, 2012. DOI: 10.1115/1.4005656

[10] J. Qiao, J. Shang, and A. Goldenberg, "Development of inchworm in-pipe robot based on self-locking mechanism", *IEEE/ASME Transactions on Mechatronics*, Vol. 18, Iss. 2, pp. 799-806, 2013. DOI: 10.1109/TMECH.2012.2184294

[11] Y. Liu, B. Lim, J. W. Lee *et al.*, "Steerable dry adhesive linkage-type wall-climbing robot", *Mechanism and Machine Theory*, Vol. 153, 2020, 103987. DOI: 10.1016/j.mechmachtheory.2020.103987

[12] K. Seo, S. Cho, T. Kim, H. S. Kim, and J. Kim, "Design and stability analysis of a novel wall-climbing robotic platform (ROPE RIDE)", *Mechanism and Machine Theory*, Vol. 70, 2013, pp. 189-208. DOI: 10.1016/j.mechmachtheory.2013.07.012

[13] T. Maneewarn and B. Maneechai, "Design of pipe crawling gaits for a snake robot", *Proceedings of the IEEE International Conference on Robotics and Biomimetics (ROBIO)*, Bangkok, Thailand, 2009, pp. 1-6. DOI: 10.1109/ROBIO.2009.4912970

[14] I. Virgala, M. Kelemen, P. Bozek *et al.*, "Investigation of snake robot locomotion possibilities in a pipe, *Symmetry*, Vol. 12, Iss. 6, pp. 1-25, 2020. DOI: 10.3390/sym12060939

[15] Z. Wang, Z. Deng, and P. Lei, "Research on technology of pipeline detection robot based on spiral propulsion", *Proceedings of the 14th International Conference on Intelligent Robotics and Applications, ICIRA 2021*, Yantai, China, 22-25 October, 2021, Part IV, pp. 67-78, 2021. DOI: 10.1007/978-3-030-89092-6_7

[16] A. Kakogawa and S. Ma, "Mobility of an in-pipe robot with screw drive mechanism inside curved pipes", *Proceedings of the IEEE International Conference on Robotics and Biomimetics*, Tianjin, China, 14-18 December, 2010, pp. 1530-1535. DOI: 10.1109/ROBIO.2010.5723557

[17] D. Liu and J. Lu, "Dynamic characteristics of two-mass inertial pipeline robot driven by noncircular gears", *Proceedings of the 14th International Conference on Intelligent Robotics and Applications, ICIRA 2021*, Yantai, China, 22-25 October, 2021, Part IV, pp. 79-90, 2021. DOI: 10.1007/978-3-030-89092-6_8

[18] C. Lee, M. Kim, Y. J. Kim *et al.*, "Soft robot review", *International Journal of Control Automation and Systems*, Vol. 15, pp. 3-15, 2017. DOI: 10.1007/s12555-016-0462-3

[19] A. Firouzeh and J. Paik, "Grasp mode and compliance control of an under-actuated origami gripper using adjustable stiffness joints", *IEEE/ASME Transactions on Mechatronics*, Vol. 22, pp. 2165-2173, 2017. DOI: 10.1109/TMECH.2017.2732827

[20] Y. Almubarak and Y. Tadesse, "Twisted and coiled polymer (TCP) muscles embedded in silicone elastomer for use in soft robot", *International Journal of Intelligent Robotics and Applications*, Vol. 1, pp. 352-368, 2017. DOI: 10.1007/s41315-017-0022-x

[21] D. Bruder, C. D. Remy, and R. Vasudevan, "Nonlinear system identification of soft robot dynamics using koopman operator theory", *Proceedings of the 2019 International Conference on Robotics and Automation (ICRA)*, Montreal, QC, Canada, 20-24 May 2019, pp. 6244-6250. DOI: 10.1109/ICRA.2019.8793766

[22] F. Renda, V. Cacucciolo, J. Dias, and L. Seneviratne, "Discrete cosserat approach for soft robot dynamics: A new piece-wise constant strain model with torsion and shears", *Proceedings of the 2016 IEEE/RSJ International Conference on Intelligent Robots and Systems (IROS)*, Daejeon, Korea (South), 9-14 October 2016, pp. 5495-5502. DOI: 10.1109/IROS.2016.7759808

[23] C. Walsh, "Human-in-the-loop development of soft wearable robots", *Nature Reviews Materials*, Vol. 3, pp. 78-80, 2018. DOI: 10.1038/s41578-018-0011-1

[24] G. Blewitt, D. Cheneler, J. Andrew, and S. Monk, "A review of worm-like pipe inspection robots: Research, trends and challenges", *Soft Science*, Mar. 2024. DOI: 10.20517/ss.2023.49

[25] D. Fang, G. Jia, J. Wu *et al.*, "A novel worm-like in-pipe robot with the rigid and soft structure", *Journal of Bionic Engineering*, No. 6, pp. 2559-2569, 2023. DOI: 10.1007/s42235-023-00395-1

MỘT RÔ BỐT LINH HOẠT LEO ỐNG MỚI DÀNH CHO VIỆC KIỂM TRA ĐƯỜNG ỐNG

Vũ Minh Hoàn[1], Trịnh Xuân Hiệp[1], Nguyễn Văn Hoan[1]
[1]*Khoa Cơ khí, Trường Đại học Kỹ thuật Lê Quý Đôn*

Tóm tắt: Đối với rô bốt, việc bò qua các đoạn ống cong, thay đổi phương chuyển động hoặc đoạn đường ống có đường kính thay đổi để kiểm tra, khảo sát là một công việc khá khó khăn và không thể tránh khỏi. Để giải quyết vấn đề này, chúng tôi đề xuất một mô hình thiết kế rô bốt kiểm tra đường ống mới là sự kết hợp hài hòa giữa phần kết cấu cơ khí cứng vững với phần thân mềm để đảm bảo rô bốt di chuyển mềm mại và linh hoạt trong đường ống. Mô hình thiết kế cơ khí của rô bốt bao gồm bộ truyền động hướng tâm phía trước, bộ truyền động hướng trục trung tâm và bộ truyền động hướng tâm phía sau. Để hỗ trợ rô bốt bám chặt vào thành ống và tạo điểm tựa vững chắc cho rô bốt trong quá trình di chuyển, các bộ truyền chuyển động phía trước và phía sau được thiết kế với cấu trúc cơ khí cứng vững và có khả năng mở rộng đường kính theo phương hướng tâm. Bộ truyền chuyển động hướng trục trung tâm là phần thân mềm có khả năng giãn nở nhanh chóng theo phương hướng trục khi được bơm đầy không khí để giúp rô bốt di chuyển về phía trước và dễ dàng di chuyển qua các đoạn ống cong. Khả năng chuyển động mềm mại và linh hoạt của rô bốt được thể hiện rõ ràng qua các mô hình động học các cấu trúc cơ khí và mô phỏng biến dạng của phần thân mềm. Kết quả tính toán và mô phỏng sơ bộ cho thấy thiết kế rô bốt mới này cho phép rô bốt có khả năng di chuyển linh hoạt và hiệu quả trong các đoạn đường ống có đường kính thay đổi và cấu hình đa dạng.

Từ khóa: *Rô bốt leo ống; rô bốt linh hoạt; thiết kế cơ khí; mô hình động học.*

Received: 18/06/2024; Revised: 27/08/2024; Accepted for publication: 21/11/2024

❑